1	The landscape of intrinsic and evolved fluoroquinolone resistance in Acinetobacter baumannii				
2	includes suppression of drug-induced prophage replication				
3					
4					
5	Running Head: Antibiotic resistance modulation of prophage induction				
6					
7	Edward Geisinger, ^{a, c} Germán Vargas-Cuebas, ^a * Nadav J. Mortman, ^a Sapna Syal, ^a Elizabeth L.				
8	Wainwright, ^c David Lazinski, ^a Stephen Wood, ^b Zeyu Zhu, ^b Jon Anthony, ^b Tim van Opijnen, ^b				
9	Ralph R. Isberg ^a #				
10					
11	^a Department of Molecular Biology and Microbiology, Tufts University School of Medicine,				
12	Boston, Massachusetts, USA				
13	^b Department of Biology, Boston College, Chestnut Hill, Massachusetts, USA				
14	^c Department of Biology, Northeastern University, Boston, Massachusetts, USA				
15					
16	#To whom correspondence should be addressed (<u>ralph.isberg@tufts.edu</u>)				
17	*Present address: Department of Microbiology and Immunology, Emory University School of				
18	Medicine, Atlanta, Georgia, USA				
19					
20					
21	Abstract word count: 396 (Abstract section: 248; Importance section: 148)				
22	Text word count: 5,979				

23 Abstract

24 The emergence of fluoroquinolone resistance in nosocomial pathogens has restricted the clinical 25 efficacy of this antibiotic class. In Acinetobacter baumannii, the majority of clinical isolates 26 now show high-level resistance due to mutations in gyrA (DNA gyrase) and parC (Topo IV). To 27 investigate the molecular basis for fluoroquinolone resistance, an exhaustive mutation analysis 28 was performed in both drug sensitive and resistant strains to identify loci that alter the sensitivity 29 of the organism to ciprofloxacin. To this end, parallel fitness tests of over 60,000 unique 30 insertion mutations were performed in strains with various alleles in genes encoding the drug 31 targets. The spectrum of mutations that altered drug sensitivity was found to be similar in the 32 drug sensitive and double mutant gyrAparC background having resistance alleles in both genes. 33 In contrast, introduction of a single gyrA resistance allele, resulting in preferential poisoning of 34 Topo IV by ciprofloxacin, led to extreme alterations in the insertion mutation fitness landscape. 35 The distinguishing feature of preferential Topo IV poisoning was induction of DNA synthesis in 36 the region of two endogenous prophages, which appeared to occur *in situ*. Induction of the 37 selective DNA synthesis in the gyrA background was also linked to enhanced activation of SOS 38 response and heightened transcription of prophage genes relative to that observed in either the 39 WT or gyrAparC double mutants. Therefore, the accumulation of mutations that result in the 40 stepwise evolution of high ciprofloxacin resistance is tightly connected to suppression of 41 hyperactivation of the SOS response and endogenous prophage DNA synthesis.

42

43 **Importance**

44 Fluoroquinolones have been extremely successful antibiotics. Their clinical efficacy derives 45 from the ability to target multiple bacterial enzymes critical to DNA replication, the 46 topoisomerases DNA gyrase and Topo IV. Unfortunately, mutations lowering drug affinity for 47 both enzymes are now widespread, rendering these drugs ineffective for many pathogens. To 48 undermine this form of resistance, we sought to understand how bacteria with target alterations 49 differentially cope with fluoroquinolone exposures. We studied this problem in the nosocomial 50 pathogen A. baumannii, which causes resistant, life-threating infections. Employing genome-51 wide approaches, we uncovered numerous pathways that could be exploited to lower 52 fluoroquinolone resistance independently of target alteration. Remarkably, fluoroquinolone 53 targeting of Topo IV in specific mutants caused dramatic prophage hyperinduction, a response 54 that was muted in strains with DNA gyrase as the primary target. This work demonstrates that 55 resistance evolution via target modification can profoundly modulate the antibiotic stress 56 response, revealing potential resistance-associated liabilities. 57

58

59 Introduction

60 *Acinetobacter baumannii* is a frequent cause of multidrug resistant infections in hospitals 61 and has been labeled a pathogen of critical priority for new drug development (1). This pathogen 62 class has rapidly evolved a broad array of drug resistance mechanisms, limiting the usefulness of 63 many widely-used antibiotics. A prime example is the fluoroquinolone class of antibiotics. These 64 drugs are widely used to treat infections caused by a range of Gram-negative and Gram-positive 65 bacteria, but they have been rendered obsolete against most *A. baumannii* isolates due to 66 extremely high frequencies of resistance (2-4). Understanding how *A. baumannii* and related

bacteria withstand treatment with fluoroquinolone antibiotics has the potential to lead tostrategies to reverse or bypass resistance.

69	Fluoroquinolones inhibit DNA replication in bacteria by targeting two enzymes essential				
70	for DNA synthesis, the type II topoisomerases DNA gyrase (gyrAB genes) and topoisomerase IV				
71	(Topo IV, <i>parCE</i>). These enzymes modulate DNA topology to maintain negative DNA				
72	supercoiling (DNA gyrase) or decatenate newly replicated DNA (Topo IV), and in so doing,				
73	break and religate DNA. Binding of fluoroquinolones to these enzymes traps them in an				
74	intermediate state that is bound to cleaved DNA, resulting in double-strand DNA breaks, blocked				
75	replication fork progression and, at high drug concentrations, cell death (5).				
76	Acquired resistance to fluoroquinolones commonly arises through stepwise mutations				
77	that disrupt the ability of the drug to bind its preferred target enzymes. In Gram-negative bacteria				
78	including A. baumannii, these mutations typically arise first in gyrA, encoding the GyrA subunit				
79	of DNA gyrase which is the more sensitive of the two enzyme targets (6). In the presence of				
80	resistant GyrA, the less sensitive Topo IV (encoded by <i>parC</i>) becomes the target and the site of				
81	second-step resistance mutations. In addition to target site alterations, acquisition of mutations				
82	that upregulate drug efflux pumps or accessory genes that allow drug modification enable				
83	bacteria to develop fluoroquinolone resistance (7). A large fraction of A. baumannii isolates				
84	harbor target-site mutations in $gyrA$ and $parC$ (8, 9) and mutations causing overproduction of				
85	one or more RND-class efflux systems that act on fluoroquinolone drugs (AdeABC, AdeFGH,				
86	AdeIJK (10-12)).				
87	Acquired resistance mechanisms generally act in combination with intrinsic resistance				

Acquired resistance mechanisms generally act in combination with intrinsic resistance
strategies in a cumulative manner to raise the amount of fluoroquinolone antibiotic required to
block bacterial growth. Regulated production of native efflux pumps contributes to intrinsic

90 fluoroquinolone resistance in many bacteria (13). Of the RND systems in A. baumannii, native 91 levels of AdeIJK in wild-type (WT) strains lacking acquired mutations have been shown to 92 provide intrinsic resistance to fluoroquinolones (12). Whether regulated production of other 93 efflux systems provides intrinsic fluoroquinolone resistance is less clear. 94 Another major strategy for intrinsic fluoroquinolone resistance is activation of DNA 95 damage repair pathways (14). DNA lesions caused by fluoroquinolone intoxication are processed 96 to single-stranded DNA and subsequently induce the SOS repair response, resulting in de-97 repression of many genes involved in DNA recombination and repair (15). Knockout mutations 98 in a variety of DNA repair genes result in increased fluoroquinolone susceptibility in several 99 species (14-24). In certain cases, the SOS response also induces mobile genetic elements that 100 carry antibiotic resistance or toxin genes, potentially influencing the spread of resistance or 101 virulence traits (25). The A. baumannii SOS repair response is non-canonical, lacking clear 102 orthologs of many major players in other systems (26) and is characterized by a phenotypically 103 variable response within cell populations (27). Inactivation of RecA, a central protein mediating 104 DNA recombinational repair and SOS induction, or the RecBCD Exonuclease V complex 105 responsible for double-strand break repair, greatly raises fluoroquinolone sensitivity in A. 106 baumannii (28, 29). The role of the SOS response and other DNA repair systems, however, in 107 the development of antibiotic resistance in this organism is largely unknown. 108 In this study, we present the results of a comprehensive screen for determinants of 109 intrinsic resistance to the fluoroquinolone antibiotic ciprofloxacin in A. baumannii. We 110 hypothesized that the ciprofloxacin resistome varies depending on the drug target (DNA gyrase 111 or Topo IV) that is preferentially poisoned, which is determined by possession of WT or resistant 112 versions of the enzymes. We therefore performed parallel screens with isogenic A. baumannii

strains containing sensitive or resistant *gyrA* and *parC* alleles to uncover the influence of target selectivity on the intrinsic resistance landscape. This analysis led to the surprising discovery that endogenous prophage activation by fluoroquinolones shows dramatic dependence on the availability of a sensitive *parC* allele.

117

118

119 Results

120 Identification of Acinetobacter baumannii loci that confer altered sensitivity to 121 ciprofloxacin. As part of a largescale effort to characterize the molecular nature of intrinsic 122 resistance of Acinetobacter baumannii to antimicrobials, we identified the entire spectrum of 123 insertion mutations that cause altered sensitivity to the fluoroquinolone antibiotic ciprofloxacin 124 during growth in bacteriological culture. A number of studies have demonstrated that mutations 125 that cause antibiotic hypersensitization in strain backgrounds lacking demonstrable resistance 126 loci exhibit these effects independently of whether there are target site resistance mutations or 127 antibiotic-inactivating enzymes present in the strains being interrogated (20, 30). We wanted to 128 test this model by first identifying loci that confer intrinsic resistance in a strain background 129 having intact drug targets, and then comparing them with intrinsic resistance loci identified in 130 strains having drug target mutations in DNA gyrase or Topo IV. For this work, we will refer to 131 lesions resulting in lowered resistance to the antibiotic as ciprofloxacin-hypersensitizing 132 mutations in each strain background, and the genes harboring these mutations as loci of 133 hypersensitization.

134To identify ciprofloxacin hypersensitization loci, ciprofloxacin concentrations below the135minimal inhibitory concentration (MIC) (Table 1) were identified that resulted in growth rates of

A. baumannii ATCC17978 in rich broth that were between 60-80% of that observed without 136 137 antibiotics (Fig. 1A). Three of these concentrations were chosen for further analysis (0.05, 0.075 138 and $0.09-0.10 \mu g/ml$) to determine the relative fitness of insertion mutations when subjected to 139 each of the antibiotic stress conditions. Multiple independent Tn10 insertion pools (7 pools for 140 $0.05 \,\mu\text{g/ml}$, and 11 pools for 0.075 and 0.09-0.10 $\mu\text{g/ml}$ ciprofloxacin) having between 6,000 141 and 18,000 individual insertions (60,000 separate sites in all) were grown in broth in the 142 presence or absence of ciprofloxacin for approximately 8 generations. DNA samples taken from 143 the initial time point prior to growth (t_1) and the final timepoint after 8 generations growth (t_2) 144 were prepared from each of the pools. The insertion sites were then amplified preferentially and 145 subjected to high density sequencing, followed by determining the relative fitness of each 146 insertion mutant based on density of reads (Materials and Methods; Data Set S1). Using 147 accepted strategies, the fitness of each insertion mutant strain was calculated relative to the entire 148 pool (31). To standardized results across experiments, fitness values were normalized to 149 insertions found in 18 neutral sites located in pseudogenes or endogenous transposon-related 150 genes throughout the genome ("neutral" mutants), to allow an accurate quantitation of the 151 representation of mutants relative to control insertions predicted to have no effect on growth 152 (32). The normalized data from the individual insertion mutations were aggregated for each 153 gene to calculate a mean fitness level for the entire spectrum of mutations found within a 154 particular gene. The complete datasets were then displayed on an individual gene level as the growth rate changes for mutations relative to the growth rate of the entire pool (Fig. 1B). 155 Candidate mutants were identified that showed lower (hypersensitizing loci) or higher fitness 156 157 levels based on the criteria that the False Discovery Rate (FDR) q value was <0.05, a change in

fitness (W_{diff}) was >10%, and fitness value was derived from at least 3 independent insertion mutants ((33); Materials and Methods).

160 Small increases in the dose of ciprofloxacin greatly increased the spectrum of 161 ciprofloxacin hypersensitivity loci (Fig. 1B; black). At a dose causing approximately 20% 162 growth inhibition, mutations in only 10 genes passed the criteria for lower fitness relative to the 163 rest of the pool in the presence of the drug. These included insertions in: two genes involved in 164 double strand break repair (recB and ruvA, encoding subunits of exonuclease V and the Holiday 165 junction helicase); the major egress pump which is often found overproduced in clinical strains 166 having high level fluoroquinolone resistance (*adeIJK*); and *ctpA*, a periplasmic protease shown 167 to be a target of mutations that augment β -lactam resistance in strains lacking the *bfmRS* global 168 regulatory system (34) (Data Set S1). Increasing the drug dose had two effects on expanding the 169 spectrum of hypersensitivity loci. First, although the number of hypersensitivity loci that 170 contribute to the enzymology of DNA repair increased from 2 members to 20 in the high dose 171 regimen, this expansion largely involved hitting additional subunits of the same complexes or 172 backup systems of the enzymes identified in the low dose regimen (*recBCD*, *sbcCD*, *ruvABC*) 173 (Data Set S1). This emphasizes the importance of protecting against double strand breaks caused 174 by fluoroquinolone-poisoned DNA gyrase (35). Secondly, increasing dose resulted in 175 hypersensitivity loci in cell envelope integrity proteins, additional protein-processing enzymes, 176 and a MATE class proton-driven efflux pump (*abeM*) shown to export ciprofloxacin and other 177 antibiotic compounds when cloned in E. coli (36) (Data Set S1; Fig. 1C). Interestingly, 178 increasing the drug dose did not implicate the two other major RND efflux systems in protecting 179 from ciprofloxacin stress even though they are known to provide low-level resistance after 180 overproduction (12). This may be explained by the fact that the *adeIJK* system is the only RND

egress pump known to have a high basal level of expression in WT strains lacking acquired
resistance mutations, while the inducing signals for the other systems have not been identified
(12). Strikingly, at the higher drug doses, mutations in *adeN*, which encodes the negative
regulator of *adeIJK*, increased the fitness of *A. baumannii* relative to the rest of the pool (Data
Set S1). These data argue strongly that the primary efflux pumps involved in intrinsic protection
from fluoroquinolone stress are AdeIJK and AbeM.

187 In addition to hypersensitivity loci, mutations were identified at the highest drug dose that 188 resulted in increased fitness relative to the insertion pool (Fig. 1B and C, Data Set S1). The 189 mutations that most frequently increased fitness targeted nonessential components of the protein 190 translation machinery, particularly enzymes that post-translationally modify tRNA, rRNA and 191 assembly of ribosomal protein complexes. That disruption of this circuit is tightly associated 192 with increased drug resistance is consistent with studies showing that a spectrum of antibiotic 193 resistant isolates in different species evolve mutations causing slowed translation rate (37, 38). 194 The results are also consistent with a study demonstrating that lowering ribosomal synthesis 195 increases resistance to ciprofloxacin by restoring an optimal balance between protein and DNA 196 synthesis levels during DNA stress (39)). Most notable among the insertions identified were 197 those in *gidA*, which is part of a complex involved in 5-methylaminomethyl-2-thiouridine 198 $(mnm^{5}s^{2}U34)$ modification of tRNAs (Data Set S1; (40)). We have previously identified this 199 gene as an additional target of mutations bypassing drug hypersensitivity resulting from loss of 200 *bfmRS* (34), indicating the tight connection between mutations in this gene and drug resistance. 201 Deletion mutants have drug sensitivities predicted by Tn-seq. Targeted deletion or 202 null mutations were isolated in nonessential genes predicted to have altered drug sensitivity in

203 the presence of ciprofloxacin. The mutations were chosen based on their fitness in the Tn-seq

204 analysis, the magnitude of the effects predicted, and differing functional categories (Fig. 1C). For 205 instance, mutations in the egress pump-encoding adeIJK showed extremely poor fitness and 206 were rarely recovered after growth in ciprofloxacin (Fig. 2A). Similarly, the insertions in *ctpA* 207 showed very low fitness. In contrast, although ciprofloxacin treatment lowered fitness for 208 mutants lacking the penicillin binding protein PBP1A, these mutations clearly had weaker effects 209 in the Tn-seq analysis. When this set of targeted mutants was analyzed further, loss of *adeIJK*, 210 recN, ctpA and pbp1A all resulted in heightened drug sensitivity (Fig. 2B). In contrast, deletion 211 of gidA-encoded tRNA modification enzyme resulted in enhanced fitness in the presence of 212 ciprofloxacin, with increased yields in broth cultures exposed to $0.15 \,\mu\text{g/ml}$ of antibiotic (Fig. 213 2B).

214 Identification of loci that result in altered ciprofloxacin sensitivity in A. baumannii 215 target site mutants. A majority of the current clinical isolates of A. baumannii are resistant to 216 fluoroquinolones, and these isolates commonly have the gyrA(S81L) and parC(S84L) target site 217 mutations that lower the affinity for these antibiotics (41). To determine the spectrum of 218 insertions that cause altered sensitivity to ciprofloxacin in strains having resistance alleles, gyrA(S81L) (hereafter referred to as $gyrA^{R}$) and gyrA(S81L) parC(S84L) (referred to as $gyrA^{R}$) 219 220 $parC^{R}$) mutants were generated, and each strain was subjected to Tn10 mutagenesis. Pools 221 totaling more than 70,000 insertion mutations were constructed in each background. Insertion 222 pools were challenged with ciprofloxacin, using drug concentrations below the MIC (Table 1) that resulted in 30-40% growth inhibition for each strain $(1.1 \mu g/ml \text{ for } gyrA^R; 13-14 \mu g/ml \text{ for})$ 223 224 $gyrA^{R} parC^{R}$ double mutant; Fig. 3A). The spectrum of insertions that resulted in hypersensitivity to ciprofloxacin in the $gyrA^{R} parC^{R}$ double mutant strain backgrounds was very 225 226 similar to the WT (Fig. 3C,D). In fact, almost every ciprofloxacin hypersensitive locus in the

227 double mutant background was identified previously in the WT (green circles, Fig. 3C; Data Sets 228 S1 and S3). In addition, there was a number of hypersensitivity loci identified in the WT pools 229 that did not pass the discovery criteria in the double mutant (FDR<0.05; W_{diff}>0.1). A number of these below-threshold candidates in the $gyrA^{R} parC^{R}$ double mutant strain background encoded 230 231 subunits of the proteins identified as ciprofloxacin-hypersensitive loci (green circles, Fig. 3C; 232 Data Set S3). These results are similar to what we had observed in our graded series of drug 233 treatments of insertion pools in the WT strain, indicating that the results from the WT strain and 234 the drug resistant double mutant are largely the same.

The results from the $gyrA^{R}$ single mutant background, however, diverged greatly from the 235 WT and the $gyrA^{R} parC^{R}$ double mutant (Fig. 3E). A large fraction of insertions were identified 236 237 that altered drug sensitivity to ciprofloxacin, with a surprising number showing increased fitness 238 during drug exposure (Fig. 3E). Over 40 of the insertions that exhibited increased fitness were 239 located in putative prophage genes (blue and yellow circles, Fig. 3E; Fig. 3F) from two of the 240 three predicted phages integrated into the bacterial chromosome (Fig. 3B; Data Set S2). No such fitness changes were seen in the WT (Fig. S2, Data Set S1) or $gyrA^{R} parC^{R}$ double mutant (Fig. 241 242 3C, Data Set S3). To analyze this result further, the normalized fitness of mutations in each gene 243 was plotted as a function of position on the chromosome. In the absence of antibiotic, there was 244 no clear positional effect of altered fitness levels along the length of the chromosome (Fig. 3G). 245 In contrast, in the presence of antibiotic, there was an apparent increase in fitness levels centered within chromosomal locations harboring prophages P1 and P3 in the $gyrA^{R}$ single mutant (Fig. 246 247 3G). Although some of this effect could be explained by loss of prophage gene function 248 resulting in enhanced fitness, insertions in chromosomal regions near, but outside, the prophage 249 boundaries similarly showed apparent increases in fitness relative to the rest of the chromosomal

insertions (Figs. 3G and H). As fitness levels are measured by counting the number of reads in
specific regions of DNA, this phenomenon is consistent with selective local amplification of
chromosomal material that initiates within these prophages, extending outward from the
integration sites into nearby DNA regions.

254 Two prophage regions are selectively amplified in response to ciprofloxacin in the 255 single $gyrA^{R}$ mutant. We next tested the model that there is induction of DNA synthesis in the 256 region surrounding two of the chromosomally-located prophage clusters. Purified single colonies from the WT, $gyrA^{R}$, and $gyrA^{R}parC^{R}$ double mutant strains were grown in broth culture for 3.5 257 258 hours in the presence of four different concentrations of ciprofloxacin that ranged from 30-80% 259 growth inhibition and compared to bacteria grown in the absence of drug (Fig. 4A). DNA was 260 then prepared from each of the cultures and subjected to whole genome sequencing using an 261 average read length of 100 bp. The density of these individual short reads was plotted as a 262 function of the chromosomal coordinates, to identify regions of chromosomal DNA that were selectively amplified in the presence of drug (Fig. 4B). Analysis of the gyrA^R single mutant 263 264 showed hyperamplification of prophages 1 and 3, with read density in the prophage regions 265 observed as a function of drug concentration. In contrast, there was little evidence of this selective amplification in the WT strain, while the $gyrA^{R}parC^{R}$ largely reversed these effects. 266 267 Consistent with the Tn-seq data, there was amplification of DNA extending beyond the 268 prophage-chromosomal DNA junction, indicating that drug-driven DNA synthesis was initiated 269 in situ and continued beyond the ends of the prophages into adjacent chromosomal DNA (Fig. 270 4C). We conclude that in a $gyrA^R$ background, selective blockage of the *parC*-encoded Topo IV 271 protein resulted in DNA synthesis induction in these two prophage regions.

To determine if transcription of prophage genes is specifically amplified in the $gvrA^R$ 272 273 mutant relative to the WT, the two strains were grown in triplicate cultures in two concentrations 274 of antibiotic for 3.5 hours that gave between 40-70% growth inhibition over approximately 7 275 generations (Fig. 5A). The cells were then extracted, subjected to RNAtag-seq analysis (42), and 276 the ratio of transcription for each gene in the presence/absence of ciprofloxacin was displayed as 277 a function of chromosomal map position (Fig. 5B, Data Set S4). There was preferential 278 amplification of transcription of prophage genes in the presence of antibiotic treatment in both 279 strain backgrounds (Fig. 5B). Furthermore, transcription was hyperactivated in all three 280 prophages, including prophage 2 which showed no evidence of preferential DNA amplification 281 (compare Figs 4B and 5B). Higher expression levels were observed with prophage genes in the 282 $gyrA^{R}$ single mutant compared to WT (Fig. 5B), and these levels were also apparent when directly comparing transcription in WT and $gyrA^{R}$ after ciprofloxacin treatment (Fig. S3). In 283 284 $gyrA^{R}$ -single mutants, enhanced expression in response to ciprofloxacin extended beyond the 285 prophage-chromosomal DNA junctions with prophage 1 and to some extent with prophage 3 286 (Fig. 5C and S3), consistent with increased DNA template availability partially contributing to 287 heightened transcription in this strain background. Hyperexpression in response to ciprofloxacin 288 terminated at the prophage-chromosomal DNA junctions with prophage 2, consistent with the 289 observation that this region experienced no DNA amplification (Fig. 5C). These results indicate 290 that preferential blockage of Topo IV in the single mutant results in hyperactivation of prophage 291 transcripts.

Intoxication of bacterial topoisomerase enzymes by fluoroquinolone antibiotics induces DNA damage, driving an SOS response (16, 43). We investigated the extent to which ciprofloxacin-induced hyperactivation of prophage gene expression coincided with SOS

295 response induction, and whether gyrA or parC resistance alleles influenced this response. Several 296 genes associated with the SOS response (27, 43, 44) showed heightened transcription as a 297 consequence of ciprofloxacin treatment (Fig. 6A). For several SOS genes, transcript induction was significantly higher in $gyrA^{R}$ compared to WT (Fig. 6A; asterisks). These included genes 298 299 adjacent to prophage-chromosomal DNA junctions (*umuC* and *umuD* paralogs) as well as those 300 not directly linked to prophages (recA, gst; Fig. 6B). RecA is a key component of the SOS 301 response that is induced by DNA damage in A. baumannii and is critical for withstanding 302 ciprofloxacin stress independent of the background resistance genotype (see Data Sets S1-S3). 303 To analyze the interplay of SOS induction by ciprofloxacin with target availability at the level of 304 single cells, we utilized a plasmid-based transcriptional fusion of the *recA* regulatory elements (promoter and 5'-untranslated region) to the fluorescent reporter mKate2 (45). WT, gvrA^R, and 305 $gvrA^{R}parC^{R}$ strains harboring the reporter fusion were cultured in the presence of graded levels 306 307 of ciprofloxacin, and reporter signal was measured in individual cells by fluorescence 308 microscopy (Materials and Methods). Increasing sub-MIC doses of ciprofloxacin caused 309 increasing degrees of induction of the *recA* reporter in all strain backgrounds (Fig. 6C). Notably, reporter activity was approximately 2-fold higher in the $gyrA^{R}$ single mutant than in the WT or 310 311 double mutant at equivalent levels of growth inhibition (Fig. 6C). Varying degrees of recA induction within populations of $gyrA^{R}$ single mutant cells were observed, and this variability 312 roughly matched that observed with WT (Fig. S4). Increased signal in the $gyrA^{R}$ strain was not 313 314 observed with a control reporter fusion to a gene that is nonresponsive to ciprofloxacin (trpBp-315 UTR) ((45), Fig 6D), indicating that the SOS transcriptional response was specifically enhanced 316 as a consequence of ciprofloxacin inhibition of Topo IV.

317

318

319 Discussion

320 In this study we exploited the dual-target nature of fluoroquinolone antibiotics to uncover how 321 resistance alleles acquired in target enzymes modulate the landscape of intrinsic resistance. 322 Using Tn-seq, we performed comprehensive screens for determinants of resistance to the 323 fluoroquinolone drug ciprofloxacin in isogeneic A. baumannii strains in which the drug 324 preferentially targets either DNA gyrase or Topo IV. We found that the spectrum of genes 325 contributing to intrinsic resistance was similar in genetic backgrounds in which both enzymes 326 were WT or in which both enzymes had lowered drug sensitivity due to well-known acquired 327 point mutations. Intrinsic resistance determinants identified in both backgrounds included the 328 AdeIJK and AbeM efflux pumps, multiple subunits of the DNA recombination and repair 329 machinery, a periplasmic protease CtpA, the cell wall transpeptidase PBP1A, and several proteins of unknown function. By contrast, interaction of ciprofloxacin with the $gyrA^{R}$ single 330 331 mutant in which Topo IV is the sensitive target dramatically altered the profile of genes that influence relative Tn-seq fitness. This altered fitness profile in $gyrA^{R}parC^{+}$ bacteria was shown 332 333 to directly reflect amplification of DNA in the vicinity of two endogenous prophages due to 334 preferential poisoning of Topo IV by ciprofloxacin. Prophage transcripts and the SOS pathway 335 were also hyperactivated as a consequence of this drug-genotype interaction, likely facilitating the initiation of synthesis of prophage DNA in the $gyrA^{R}$ strain. 336 337 Our data can be explained by the model shown in Fig. 7, if we assume that re-activation

of *A. baumannii* prophages 1 and 3 requires the function of host DNA gyrase. In WT and the gyr A^{R} par C^{R} double mutant, DNA gyrase is the effective target blocked by ciprofloxacin at growth-inhibitory, sub-MIC drug concentrations. Prophage DNA synthesis is blocked despite

341 induction of the DNA damage response and prophage gene transcription because, as postulated 342 by the model, efficient replication of the prophage genomes requires functional host gyrase (Fig. 7A and C). By contrast, in $gyrA^{R}$ bacteria, Topo IV is the preferred target of intoxication by 343 344 ciprofloxacin. This interaction causes DNA lesions that robustly stimulate the SOS pathway and 345 prophage transcription; further, host DNA gyrase is available to facilitate prophage genome replication because the GyrA S81L $(gyrA^R)$ variant is resistant to the intermediate concentrations 346 347 of ciprofloxacin required for Topo IV poisoning (Fig. 7B). Therefore, the presence of the single 348 $gyrA^{R}$ resistance generates a liability that is not observed in other strains, resulting from the 349 induction of potentially lethal prophage replication in the presence of fluoroquinolones.

350 The central assumption of the model is plausible based on analogy with several other 351 bacteriophage systems that have been shown to require host DNA gyrase for replication. Gyrase 352 inhibitors (quinolones or aminocoumarins) inhibit phage DNA replication during lytic growth 353 after infection (46-51), and disrupt induction of replicative transposition in Mu lysogens (52). 354 Moreover, host gyrase is required for propagation of replication forks within supercoiled DNA 355 substrates in reconstituted systems modeling phage lambda replication (53, 54). The importance 356 of this enzyme class for replication of A. baumannii strain 17978 prophages is emphasized by the 357 fact that they do not encode type II topoisomerases which are often encoded by bacteriophages to 358 bypass a requirement for the host enzymes (55, 56).

An alternative model is that at the sub-MIC drug doses resulting in equivalent growth inhibition, gyrase poisoning results in DNA lesions that do not stimulate the SOS response above the threshold required for efficient prophage induction, in contrast to lesions caused by Topo IV poisoning. Arguing against this model are the observations that transcription of the SOS response gene *recA* and genes from all three prophages are strongly induced (25-50 fold, Figs. 5B and 6C)

364 above baseline in WT cells, and Tn-seq fitness results showing the relatively similar importance 365 of DNA damage repair enzymes across all strain backgrounds (Data Sets S1-S3). We showed 366 that Topo IV intoxication stimulated the SOS pathway to a greater extent than that caused by 367 gyrase poisoning, potentially contributing to the robust activation of prophages. This is 368 consistent with previous findings that Topo IV and gyrase intoxication can be distinguished by 369 several characteristics. Topo IV lesions result in slower inhibition of DNA synthesis and are 370 thought to be more readily reversed by recombinational repair, resulting in lower cytotoxicity at 371 given drug concentrations (16). These less toxic lesions could potentially expose more numerous 372 or potent signals for the SOS response that could result in prophage induction. 373 In contrast with induction of prophages 1 and 3, ciprofloxacin-induced DNA replication 374 was not observed with prophage 2 despite activation of prophage gene transcription. One 375 possible explanation is that prophage 2 is defective for DNA replication. We consider this 376 unlikely because transposon insertions were unobtainable in a phage locus (ACX60_RS10145) 377 encoding a putative Cro/Cl family repressor (Data Sets S1-S3), indicating that this prophage has 378 the potential for lytic replication in the absence of a protein controlling lysogeny maintenance. 379 Consistent with the potential of all three prophages (including prophage 2) for replication, 380 mobilized DNA corresponding to each of the three prophages was detected in phage particles 381 resulting from treatment of WT A. baumannii 17978 with mitomycin C, which damages DNA 382 directly without dependence on interactions with DNA topoisomerases (44). An alternative 383 explanation for the lack of prophage 2 DNA amplification observed with fluoroquinolone 384 treatment in our study is that its replication depends on both DNA gyrase and Topo IV. 385 The findings described here have implications for the evolution of antibiotic resistance in 386 A. baumannii and other Gram-negative organisms. They indicate that in the trajectory toward

387 high-level fluoroquinolone resistance, intermediate states with moderate-level fluoroquinolone resistance (exemplified by the $gyrA^{R}$ single mutant) are those that possess highest potential for 388 389 prophage induction during growth with continued drug exposure. Depending on the outcome of 390 phage-host interactions, prophage hyperamplification within these bacteria could impose a 391 fitness burden or could result in cell death if productive lysis ensues, representing additional 392 selective pressures to influence evolution when under stress from the inducing antibiotic. 393 Acquiring the subsequent *parC* mutation would answer this pressure and result in high-level 394 fluoroquinolone resistance. It is notable that hyperamplified and hyperexpressed DNA within or 395 adjacent to induced prophages include multiple umuCD paralogs encoding mutagenic DNA 396 polymerases (57), whose higher levels of activity could increase mutation frequency and hasten bacterial adaptation in drug-treated $gyrA^{R}$ single mutants. Moreover, these findings raise the 397 398 possibility of enhanced horizontal transfer of phage-encoded and phage-proximal genes as a consequence of fluoroquinolone- $gyrA^{R}$ interactions. The relationship between stepwise 399 400 fluoroquinolone resistance and induction of prophages by this drug class may play out differently 401 with Gram-positive organisms in which Topo IV is typically the sensitive initial target as 402 opposed to gyrase (6). If fluoroquinolone-prophage dynamics in such bacteria have features that 403 accord with the model proposed here, WT strains with two sensitive *parC* and *gyrA* alleles may 404 represent the state with higher potential for drug-induced prophage replication than derivatives 405 that have acquired single-step target-resistance mutations.

In summary, we have demonstrated that in the course of stepwise selection for high drug resistance, intermediate steps result in unexpected nodes of hypersensitivity that place both added pressure for acquisition of additional drug resistant alleles, as well as inducing the enzymatic machinery that drives acquisition of drug resistance. Future work on analysis of

- 410 proteins that modulate the survival of drug resistant mutants should uncover strategies that allow411 these variants to be targeted therapeutically.
- 412

413 Materials and Methods

- 414 Bacterial strains, growth conditions, and antibiotics. Bacterial strains used in this work are
- 415 described in Table S1. A. baumannii strains were derivatives of ATCC 17978. Bacterial cultures
- 416 were grown at 37°C in Lysogeny Broth (LB) (10 g/L tryptone, 5 g/L yeast extract, 10 g/L NaCl)
- 417 in flasks with shaking or in tubes on a roller drum. Growth was monitored by measuring
- 418 absorbance at 600nm via a spectrophotometer. LB agar was supplemented with antibiotics
- 419 [ampicillin (Amp, 50-100 μg/ml), carbenicillin (Cb, 50-100 μg/ml), kanamycin (Km, 10-20
- 420 μg/ml), mecillinam, ciprofloxacin] or sucrose as needed (Sigma Aldrich).
- 421

422 Molecular cloning and mutant construction. Oligonucleotide primers and plasmids used in this study are listed in Table S2. Single gyrAS81L ($gyrA^{R}$) and parCS84L ($parC^{R}$) point 423 424 mutations were generated by cloning the respective genomic fragments in pUC18, followed by 425 inverse PCR and self-ligation or amplification and substitution of a mutated gene fragment. In-426 frame deletions of ciprofloxacin-resistance genes were generated as described (58). Constructs 427 were subcloned in pSR47S and used to isolate A. baumannii mutants via homologous recombination with two selection steps (58). The $gyrA^{R} parC^{R}$ double mutant was isolated by 428 selection of a derivative of the $gyrA^{R}$ strain able to grow on LB agar containing 8 $\mu g/ml$ 429 430 ciprofloxacin. A pbp1a mutant (N178TfsX27) was isolated as a derivative of ATCC 17978 431 selected on LB agar containing 64 µg/ml mecillinam.

433 Antibiotic susceptibility assays. For growth curve analysis, cultures were seeded at $A_{600} =$ 434 0.003 in 100µl of broth in wells of a 96-well microtiter plate and growth monitored during 435 incubation at 37°C with orbital shaking in a Tecan M200 Pro plate reader. MIC tests were 436 performed under the conditions above using serial 2-fold dilutions of drug; the MIC was the

437 lowest drug concentration preventing growth above $A_{600} = 0.05$ after 16 hours.

438

439 Construction of transposon mutant libraries. Plasmid pDL1073 was employed for transposon mutagenesis. pDL1073 contains a Km^R Tn10 derivative, an altered target-specificity Tn10 440 441 transposase gene downstream of the phage lambda P_L promoter, a pSC101ts origin of replication, and β-lactamase (Amp^R; Fig. S1). pDL1073 does not replicate in A. baumannii at 37°C allowing 442 443 efficient detection at this temperature of transposition after delivery via electroporation. A. 444 baumannii cells (50µl) were combined with 100ng pDL1073 and electroporated via a BioRad 445 Gene Pulser (0.1cm gap length cuvette; 200Ω , 25μ F, and 1.8kV). Electroporated cells were 446 diluted with SOC broth and immediately spread onto membrane filters (0.45µm pore size) 447 overlaid on pre-warmed LB agar plates. After incubating 2 hours at 37°C, the filter membranes 448 were transferred to pre-warmed LB agar plates containing 20µg/ml Km and incubated at 37°C 449 overnight to select for transposon mutants. Bacterial colonies were lifted from the filter by 450 agitation in sterile PBS. Glycerol was added to 10% (v/v), and pooled mutant suspensions were 451 aliquoted and stored at -80°C. 11-15 independent pools each consisting of approximately 6,000-452 18,000 mutants were generated in each strain background.

453

454 **Tn-seq fitness measurements.** Transposon library aliquots were thawed, vortexed, diluted to 455 $A_{600} = 0.1$ and grown to $A_{600} = 0.2$ in LB. Cultures were then back-diluted to $A_{600} = 0.003$ in

456	10ml LB without drug or with graded concentrations of ciprofloxacin. Parallel cultures were
457	grown at 37°C for approximately 8 generations to $A_{600} = 0.5$ -1. Samples taken at the start (t ₁) and
458	end (t_2) of this outgrowth were stored at -20°C. 11 to 15 independent transposon libraries were
459	analyzed with each strain background. With WT libraries, treatments with 0.075 $\mu\text{g/ml}$ and 0.09-
460	0.1 μ g/ml ciprofloxacin were performed in parallel with the same untreated control.
461	

462 **Tn-seq Illumina library preparation.** Genomic DNA was extracted from t₁ and t₂ samples 463 (Qiagen DNeasy Kit) and quantified by a SYBR green microtiter assay. Transposon-adjacent DNA was amplified for Illumina sequencing using a modification of the NexteraTM DNA Library 464 465 Prep method (Illumina). 30ng of genomic DNA was used as input in a 10µl tagmentation 466 reaction. Reaction conditions were 55°C for 5min followed by inactivation at 95°C for 0.5min. 467 Transposon-adjacent genomic DNA was amplified by adding 40µl of PCR master mix 468 containing primers olj928 and Nextera 2A-R (0.6µM final) and Q5 High-Fidelity polymerase 469 (NEB). Reaction conditions were 98°C for 10s, 65°C for 20s, and 72°C for 1min (30 cycles), 470 followed by a final extension at 72°C for 2min. A second PCR was performed using nested, 471 indexed primers. This reaction contained 0.5μ L of the first PCR reaction, Left Tn10 indexing 472 primer (0.6μ M), Right indexing primer (0.6μ M) and Q5 polymerase in a 50µl final volume. 473 Reaction conditions were 98°C for 10s, 65°C for 20s, and 72°C for 1min (12 cycles of), followed 474 by a final extension at 72°C for 2min. A sample of the second PCR product was imaged after 475 separation on a 2% agarose/TAE gel containing SYBR Safe dye. Samples were multiplexed 476 based on signal intensity in the 250-600bp region and purified (Qiagen QIAquick). 15-20pmol of 477 DNA was used as template in a 50µl reconditioning reaction containing adapter-specific primers 478 P1 and P2 (0.6µM) and Q5 polymerase. Reaction conditions were 95°C for 1min, 0.1°C/sec ramp

479	to 64°C, 64°C for 20s, 72°C for 10min. Samples were purified (Qiagen QIAquick), followed by
480	quantification and size selection (250-600bp, Pippin HT) by the Tufts University Genomics Core
481	Facility (TUCF-Genomics). Libraries were sequenced (single-end 50bp) using custom primer
482	olk115 on a HiSeq2500 with High Output V4 chemistry at TUCF-Genomics.
483	
484	Tn-seq data analysis. Reads were demultiplexed, quality-filtered and clipped of adapters before
485	serving as input for mapping and fitness calculations (31). Reads were mapped to the A .
486	baumannii 17978-mff chromosome (NZ_CP012004) and plasmids (NC_009083, NC_009084,
487	and NZ_CP012005) using previously described parameters (59). Fitness values for each
488	transposon mutant were calculated by comparing mutant vs population-wide expansion between
489	t_1 and t_2 (31). Per-gene average fitness and SD were then computed from fitness scores for all
490	insertion mutations within a gene across multiple parallel transposon pools. Differences in
491	average gene fitness between treated and untreated conditions (W_{diff}) were considered significant
492	if they fulfilled the following 3 criteria, with minor modification from those previously described
493	(33): per-gene fitness must be calculated from at least 3 data points, the magnitude of W_{diff} must
494	be > 10%, and q value must be < 0.05 in an unpaired t-test with FDR controlled by the 2-stage
495	step-up method of Benjamini, Krieger and Yekutieli (GraphPad Prism 7). Per-insertion fitness
496	scores within a given genomic region were visualized using Integrative Genomics Viewer
497	software (60) after aggregating all scores across multiple independent transposon mutant
498	libraries using the SingleFitness Perl script (61).
499	

500 Whole-genome sequencing of individual strains subjected to ciprofloxacin. WT, $gyrA^R$, or 501 $gyrA^R parC^R$ strains were grown from single colonies to early post-exponential phase and back-

502	diluted to A_{600} 0.003. Parallel cultures were grown for 2.5 hours in the absence of treatment, or					
503	3.5 hours in the presence of ciprofloxacin treatment. DNA was extracted (Qiagen DNeasy) and					
504	Illumina sequencing libraries were amplified and sequenced as described (34). After mapping to					
505	NZ_CP012004, coverage files were generated from the resulting BAM files using deepTools,					
506	with reads normalized to counts per million (62).					
507						
508	Transcriptional profiling. Cultures were diluted to A_{600} 0.003 and grown for 2.5 hours					
509	(untreated) or 3.5 hours (ciprofloxacin treated). Cultures were mixed with an equal volume of					
510	ice-cold acetone:ethanol (1:1) and stored at -80°C. Cells were thawed and washed with TE and					
511	RNA was extracted (Qiagen RNeasy). RNA samples were diluted, combined with SUPERase-in					
512	(Invitrogen), and processed via the RNAtag-seq method (42). Illumina cDNA sequencing					
513	libraries were sequenced and reads processed as described (63). Differential expression was					
514	calculated using DESeq2 (64).					
515						
516	Fluorescence reporter assays. Strains containing pCC1 or pCC7 were cultured in the presence					
517	or absence of ciprofloxacin as in RNA-seq experiments. Cells were immobilized on agarose pads					
518	and imaged on a Leica AF6000 microscope using a 100X/1.3 objective and TX2 filtercube					
519	(excitation: BP 560/40, dichromatic mirror 595, emission: BP 645/75). MicrobeJ (65) was used					
520	to measure background-corrected mean fluorescence intensity per cell. Median cellular					
521	fluorescence intensities from populations of at least 100 bacteria were determined, and median					
522	values across multiple independent experiments were averaged.					

524	Accession Number(s). Sequencing reads analyzed in this study were deposited into SRA				
525	database as: SRP157243 (Tn-seq), PRJNA495614 (RNA-seq), and PRJNA495623 (Whole				
526	genome sequencing).				
527					
528	Acknowledgements.				
529	This work was supported by NIAID awards U01AI124302 to RRI and TVO, R21AI128328 to				
530	RRI, and F32AI098358 to EG. NSF REU Site Award #1757443 to the Northeastern University				
531	Department of Biology supported the research of ELW. We thank Carly Ching and Veronica				
532	Godoy for gift of pCC1 and pCC7, and Amy Tang for assistance with bioinformatics analysis.				
533					
534 535	References				
536 537 538 539 540	 Tacconelli E, Carrara E, Savoldi A, Harbarth S, Mendelson M, Monnet DL, Pulcini C, Kahlmeter G, Kluytmans J, Carmeli Y, Ouellette M, Outterson K, Patel J, Cavaleri M, Cox EM, Houchens CR, Grayson ML, Hansen P, Singh N, Theuretzbacher U, Magrini N, Group WHOPPLW. 2018. Discovery, research, and development of new antibiotics: the WHO priority list of antibiotic-resistant bacteria and tuberculosis. Lancet Infect Dis 				
541 542 543 544 545	 18:318-327. Warner WA, Kuang SN, Hernandez R, Chong MC, Ewing PJ, Fleischer J, Meng J, Chu S, Terashita D, English L, Chen W, Xu HH. 2016. Molecular characterization and antimicrobial susceptibility of Acinetobacter baumannii isolates obtained from two hospital outbreaks in Los Angeles County, California, USA. BMC Infect Dis 16:194. 				
546 547 548 549 550	 Kim D, Ahn JY, Lee CH, Jang SJ, Lee H, Yong D, Jeong SH, Lee K. 2017. Increasing Resistance to Extended-Spectrum Cephalosporins, Fluoroquinolone, and Carbapenem in Gram-Negative Bacilli and the Emergence of Carbapenem Non-Susceptibility in Klebsiella pneumoniae: Analysis of Korean Antimicrobial Resistance Monitoring System (KARMS) Data From 2013 to 2015. Ann Lab Med 37:231-239. 				
551 552 553 554	 Blanco N, Harris AD, Rock C, Johnson JK, Pineles L, Bonomo RA, Srinivasan A, Pettigrew MM, Thom KA, the CDCEP. 2018. Risk Factors and Outcomes Associated with Multidrug-Resistant Acinetobacter baumannii upon Intensive Care Unit Admission. Antimicrob Agents Chemother 62. 				
555 556 557 558	 Drlica K, Hiasa H, Kerns R, Malik M, Mustaev A, Zhao X. 2009. Quinolones: action and resistance updated. Curr Top Med Chem 9:981-98. Hooper DC. 1999. Mechanisms of fluoroquinolone resistance. Drug Resist Updat 2:38-55. 				

559 560	7.	Jacoby GA. 2005. Mechanisms of resistance to quinolones. Clin Infect Dis 41 Suppl 2:S120-6.
561	8.	Hujer KM, Hujer AM, Hulten EA, Bajaksouzian S, Adams JM, Donskey CJ, Ecker DJ,
562	0.	Massire C, Eshoo MW, Sampath R, Thomson JM, Rather PN, Craft DW, Fishbain JT,
563		Ewell AJ, Jacobs MR, Paterson DL, Bonomo RA. 2006. Analysis of antibiotic resistance
564		genes in multidrug-resistant Acinetobacter sp. isolates from military and civilian patients
565		treated at the Walter Reed Army Medical Center. Antimicrob Agents Chemother
566		50:4114-23.
567	9.	Valentine SC, Contreras D, Tan S, Real LJ, Chu S, Xu HH. 2008. Phenotypic and
568		molecular characterization of Acinetobacter baumannii clinical isolates from nosocomial
569		outbreaks in Los Angeles County, California. J Clin Microbiol 46:2499-507.
570	10.	Fernando D, Zhanel G, Kumar A. 2013. Antibiotic resistance and expression of
571		resistance-nodulation-division pump- and outer membrane porin-encoding genes in
572		Acinetobacter species isolated from Canadian hospitals. Can J Infect Dis Med Microbiol
573		24:17-21.
574	11.	Rumbo C, Gato E, Lopez M, Ruiz de Alegria C, Fernandez-Cuenca F, Martinez-Martinez
575		L, Vila J, Pachon J, Cisneros JM, Rodriguez-Bano J, Pascual A, Bou G, Tomas M,
576		Spanish Group of Nosocomial I, Mechanisms of A, Resistance to A, Spanish Society of
577		Clinical M, Infectious D, Spanish Network for Research in Infectious D. 2013.
578		Contribution of efflux pumps, porins, and beta-lactamases to multidrug resistance in
579		clinical isolates of Acinetobacter baumannii. Antimicrob Agents Chemother 57:5247-57.
580	12.	Yoon EJ, Chabane YN, Goussard S, Snesrud E, Courvalin P, De E, Grillot-Courvalin C.
581		2015. Contribution of resistance-nodulation-cell division efflux systems to antibiotic
582		resistance and biofilm formation in Acinetobacter baumannii. MBio 6:e00309-15.
583	13.	Poole K. 2000. Efflux-mediated resistance to fluoroquinolones in gram-negative bacteria.
584		Antimicrob Agents Chemother 44:2233-41.
585	14.	Recacha E, Machuca J, Diaz de Alba P, Ramos-Guelfo M, Docobo-Perez F, Rodriguez-
586		Beltran J, Blazquez J, Pascual A, Rodriguez-Martinez JM. 2017. Quinolone Resistance
587		Reversion by Targeting the SOS Response. MBio 8.
588	15.	Cirz RT, Chin JK, Andes DR, de Crecy-Lagard V, Craig WA, Romesberg FE. 2005.
589		Inhibition of mutation and combating the evolution of antibiotic resistance. PLoS Biol
590		3:e176.
591	16.	Khodursky AB, Cozzarelli NR. 1998. The mechanism of inhibition of topoisomerase IV
592		by quinolone antibacterials. J Biol Chem 273:27668-77.
593	17.	Mo CY, Manning SA, Roggiani M, Culyba MJ, Samuels AN, Sniegowski PD, Goulian
594		M, Kohli RM. 2016. Systematically Altering Bacterial SOS Activity under Stress Reveals
595	10	Therapeutic Strategies for Potentiating Antibiotics. mSphere 1.
596	18.	Nichols RJ, Sen S, Choo YJ, Beltrao P, Zietek M, Chaba R, Lee S, Kazmierczak KM,
597		Lee KJ, Wong A, Shales M, Lovett S, Winkler ME, Krogan NJ, Typas A, Gross CA.
598	10	2011. Phenotypic landscape of a bacterial cell. Cell 144:143-56.
599	19.	Sutherland JH, Tse-Dinh YC. 2010. Analysis of RuvABC and RecG involvement in the
600		escherichia coli response to the covalent topoisomerase-DNA complex. J Bacteriol
601	20	
602	20.	Tamae C, Liu A, Kim K, Sitz D, Hong J, Becket E, Bui A, Solaimani P, Tran KP, Yang
603		H, Miller JH. 2008. Determination of antibiotic hypersensitivity among 4,000 single-
604		gene-knockout mutants of Escherichia coli. J Bacteriol 190:5981-8.

605	21.	Urios A, Herrera G, Aleixandre V, Blanco M. 1990. Expression of the recA gene is
606		reduced in Escherichia coli topoisomerase I mutants. Mutat Res 243:267-72.
607	22.	Brazas MD, Breidenstein EB, Overhage J, Hancock RE. 2007. Role of lon, an ATP-
608		dependent protease homolog, in resistance of Pseudomonas aeruginosa to ciprofloxacin.
609		Antimicrob Agents Chemother 51:4276-83.
610	23.	Breidenstein EB, Khaira BK, Wiegand I, Overhage J, Hancock RE. 2008. Complex
611		ciprofloxacin resistome revealed by screening a Pseudomonas aeruginosa mutant library
612		for altered susceptibility. Antimicrob Agents Chemother 52:4486-91.
613	24.	van Opijnen T, Camilli A. 2012. A fine scale phenotype-genotype virulence map of a
614		bacterial pathogen. Genome Res 22:2541-51.
615	25.	Kelley WL. 2006. Lex marks the spot: the virulent side of SOS and a closer look at the
616		LexA regulon. Mol Microbiol 62:1228-38.
617	26.	Robinson A, Brzoska AJ, Turner KM, Withers R, Harry EJ, Lewis PJ, Dixon NE. 2010.
618		Essential biological processes of an emerging pathogen: DNA replication, transcription,
619		and cell division in Acinetobacter spp. Microbiol Mol Biol Rev 74:273-97.
620	27.	Macguire AE, Ching MC, Diamond BH, Kazakov A, Novichkov P, Godoy VG. 2014.
621		Activation of phenotypic subpopulations in response to ciprofloxacin treatment in
622		Acinetobacter baumannii. Mol Microbiol 92:138-52.
623	28.	Aranda J, Bardina C, Beceiro A, Rumbo S, Cabral MP, Barbe J, Bou G. 2011.
624	20.	Acinetobacter baumannii RecA protein in repair of DNA damage, antimicrobial
625		resistance, general stress response, and virulence. J Bacteriol 193:3740-7.
626	29.	Saroj SD, Clemmer KM, Bonomo RA, Rather PN. 2012. Novel mechanism for
620 627	2).	fluoroquinolone resistance in Acinetobacter baumannii. Antimicrob Agents Chemother
628		56:4955-7.
628	30.	Gallagher LA, Lee SA, Manoil C. 2017. Importance of Core Genome Functions for an
630	50.	Extreme Antibiotic Resistance Trait. MBio 8.
631	31.	van Opijnen T, Camilli A. 2013. Transposon insertion sequencing: a new tool for
632	51.	systems-level analysis of microorganisms. Nat Rev Microbiol 11:435-42.
633	32.	van Opijnen T, Bodi KL, Camilli A. 2009. Tn-seq: high-throughput parallel sequencing
	52.	for fitness and genetic interaction studies in microorganisms. Nat Methods 6:767-72.
634 625	22	6 6
635	33.	van Opijnen T, Dedrick S, Bento J. 2016. Strain Dependent Genetic Networks for
636		Antibiotic-Sensitivity in a Bacterial Pathogen with a Large Pan-Genome. PLoS Pathog
637	24	12:e1005869.
638	34.	Geisinger E, Mortman NJ, Vargas-Cuebas G, Tai AK, Isberg RR. 2018. A global
639		regulatory system links virulence and antibiotic resistance to envelope homeostasis in
640	25	Acinetobacter baumannii. PLoS Pathog 14:e1007030.
641	35.	Drlica K, Zhao X. 1997. DNA gyrase, topoisomerase IV, and the 4-quinolones. Microbiol
642	26	Mol Biol Rev 61:377-92.
643	36.	Su XZ, Chen J, Mizushima T, Kuroda T, Tsuchiya T. 2005. AbeM, an H+-coupled
644		Acinetobacter baumannii multidrug efflux pump belonging to the MATE family of
645		transporters. Antimicrob Agents Chemother 49:4362-4.
646	37.	Knauf GA, Cunningham AL, Kazi MI, Riddington IM, Crofts AA, Cattoir V, Trent MS,
647		Davies BW. 2018. Exploring the Antimicrobial Action of Quaternary Amines against
648	• -	Acinetobacter baumannii. MBio 9.
649	38.	Gomez JE, Kaufmann-Malaga BB, Wivagg CN, Kim PB, Silvis MR, Renedo N, Ioerger
650		TR, Ahmad R, Livny J, Fishbein S, Sacchettini JC, Carr SA, Hung DT. 2017. Ribosomal

651		mutations promote the evolution of antibiotic resistance in a multidrug environment. Elife			
652		6.			
653	39.	Bollenbach T, Quan S, Chait R, Kishony R. 2009. Nonoptimal microbial response to			
654		antibiotics underlies suppressive drug interactions. Cell 139:707-18.			
655	40.	Shippy DC, Fadl AA. 2015. RNA modification enzymes encoded by the gid operon:			
656		Implications in biology and virulence of bacteria. Microb Pathog 89:100-7.			
657	41.	Hujer KM, Hujer AM, Endimiani A, Thomson JM, Adams MD, Goglin K, Rather PN,			
658		Pennella TT, Massire C, Eshoo MW, Sampath R, Blyn LB, Ecker DJ, Bonomo RA. 2009.			
659		Rapid determination of quinolone resistance in Acinetobacter spp. J Clin Microbiol			
660		47:1436-42.			
661	42.	Shishkin AA, Giannoukos G, Kucukural A, Ciulla D, Busby M, Surka C, Chen J,			
662		Bhattacharyya RP, Rudy RF, Patel MM, Novod N, Hung DT, Gnirke A, Garber M,			
663		Guttman M, Livny J. 2015. Simultaneous generation of many RNA-seq libraries in a			
664		single reaction. Nat Methods 12:323-5.			
665	43.	Simmons LA, Foti JJ, Cohen SE, Walker GC. 2008. The SOS Regulatory Network.			
666		EcoSal Plus 3.			
667	44.	Hare JM, Ferrell JC, Witkowski TA, Grice AN. 2014. Prophage induction and			
668		differential RecA and UmuDAb transcriptome regulation in the DNA damage responses			
669		of Acinetobacter baumannii and Acinetobacter baylyi. PLoS One 9:e93861.			
670	45.	Ching C, Gozzi K, Heinemann B, Chai Y, Godoy VG. 2017. RNA-Mediated cis			
671		Regulation in Acinetobacter baumannii Modulates Stress-Induced Phenotypic Variation.			
672		J Bacteriol 199.			
673	46.	Erb ML, Kraemer JA, Coker JK, Chaikeeratisak V, Nonejuie P, Agard DA, Pogliano J.			
674		2014. A bacteriophage tubulin harnesses dynamic instability to center DNA in infected			
675		cells. Elife 3.			
676	47.	Constantinou A, Voelkel-Meiman K, Sternglanz R, McCorquodale MM, McCorquodale			
677		DJ. 1986. Involvement of host DNA gyrase in growth of bacteriophage T5. J Virol			
678		57:875-82.			
679	48.	Alonso JC, Sarachu AN, Grau O. 1981. DNA gyrase inhibitors block development of			
680		Bacillus subtilis bacteriophage SP01. J Virol 39:855-60.			
681	49.	Alcorlo M, Salas M, Hermoso JM. 2007. In vivo DNA binding of bacteriophage GA-1			
682		protein p6. J Bacteriol 189:8024-33.			
683	50.	Kreuzer KN, Cozzarelli NR. 1979. Escherichia coli mutants thermosensitive for			
684		deoxyribonucleic acid gyrase subunit A: effects on deoxyribonucleic acid replication,			
685		transcription, and bacteriophage growth. J Bacteriol 140:424-35.			
686	51.	Itoh T, Tomizawa JI. 1977. Involvement of DNA gyrase in bacteriophage T7 DNA			
687		replication. Nature 270:78-80.			
688	52.	Sokolsky TD, Baker TA. 2003. DNA gyrase requirements distinguish the alternate			
689		pathways of Mu transposition. Mol Microbiol 47:397-409.			
690	53.	Dodson M, Echols H, Wickner S, Alfano C, Mensa-Wilmot K, Gomes B, LeBowitz J,			
691		Roberts JD, McMacken R. 1986. Specialized nucleoprotein structures at the origin of			
692		replication of bacteriophage lambda: localized unwinding of duplex DNA by a six-			
693		protein reaction. Proc Natl Acad Sci U S A 83:7638-42.			
694	54.	Mensa-Wilmot K, Seaby R, Alfano C, Wold MC, Gomes B, McMacken R. 1989.			
695		Reconstitution of a nine-protein system that initiates bacteriophage lambda DNA			
696		replication. J Biol Chem 264:2853-61.			

697	55.	Kreuzer KN. 1998. Bacteriophage T4, a model system for understanding the mechanism					
698	of type II topoisomerase inhibitors. Biochim Biophys Acta 1400:339-47.						
699	56. Huang WM, Wei LS, Casjens S. 1985. Relationship between bacteriophage T4 and T6						
700	DNA topoisomerases. T6 39-protein subunit is equivalent to the combined T4 39- and						
701	60-protein subunits. J Biol Chem 260:8973-7.						
702	57. Sutton MD, Smith BT, Godoy VG, Walker GC. 2000. The SOS response: recent insights						
703		into umuDC-dependent mutagenesis and DNA damage tolerance. Annu Rev Genet					
704		34:479-497.					
705	58.	Geisinger E, Isberg RR. 2015. Antibiotic modulation of capsular exopolysaccharide and					
706	50.	virulence in Acinetobacter baumannii. PLoS Pathog 11:e1004691.					
707	59.	Carter R, Wolf J, van Opijnen T, Muller M, Obert C, Burnham C, Mann B, Li Y, Hayden					
708	071	RT, Pestina T, Persons D, Camilli A, Flynn PM, Tuomanen EI, Rosch JW. 2014.					
709		Genomic analyses of pneumococci from children with sickle cell disease expose host-					
710		specific bacterial adaptations and deficits in current interventions. Cell Host Microbe					
711		15:587-599.					
712	60.	Robinson JT, Thorvaldsdottir H, Winckler W, Guttman M, Lander ES, Getz G, Mesirov					
713	00.	JP. 2011. Integrative genomics viewer. Nat Biotechnol 29:24-6.					
714	61.	McCoy KM, Antonio ML, van Opijnen T. 2017. MAGenTA: a Galaxy implemented tool					
715	for complete Tn-Seq analysis and data visualization. Bioinformatics 33:2781-2783.						
716	62. Ramirez F, Dundar F, Diehl S, Gruning BA, Manke T. 2014. deepTools: a flexible						
717	platform for exploring deep-sequencing data. Nucleic Acids Res 42:W187-91.						
718	63.	Jensen PA, Zhu Z, van Opijnen T. 2017. Antibiotics Disrupt Coordination between					
719	05.	Transcriptional and Phenotypic Stress Responses in Pathogenic Bacteria. Cell Rep					
720		20:1705-1716.					
721	64.	Love MI, Huber W, Anders S. 2014. Moderated estimation of fold change and dispersion					
722	0.11	for RNA-seq data with DESeq2. Genome Biol 15:550.					
723	65.						
724		cell detection and quantitative analysis. Nat Microbiol 1:16077.					
725	66.	Arndt D, Grant JR, Marcu A, Sajed T, Pon A, Liang Y, Wishart DS. 2016. PHASTER: a					
726		better, faster version of the PHAST phage search tool. Nucleic Acids Res 44:W16-21.					
727		·····, ·······························					
728							
729	Figu	re Legends.					
	U						
730							
731	Fig. 1	Fig. 1. Tn-seq quantification of genome-wide mutant fitness in A. baumannii (gyr A^{WT} and					
732	parC	^{WT}) during growth with sub-MIC ciprofloxacin. (A) Graded concentrations of					
_							
733	cipro	ciprofloxacin cause increasing degrees of growth inhibition. Transposon mutant libraries					

constructed in a strain background harboring WT alleles of the *gyrA* and *parC* genes were grown

735 with ciprofloxacin at the concentrations indicated. Growth rate relative to untreated control was 736 determined from bacterial density measurements. Data points show average \pm SD (n \geq 2). (B) 737 Tn-seq fitness profiles during ciprofloxacin challenge. Mutant pools were grown with or without 738 the indicated ciprofloxacin concentration and average fitness for each chromosomal gene was 739 calculated. Change in fitness resulting from ciprofloxacin treatment relative to untreated controls 740 is plotted against significance score resulting from parallel t-tests. Data points shaded in black 741 indicate gene knockouts causing significant alteration in fitness during drug challenge (W_{treated}-742 $W_{untreated}$ had a magnitude > 0.1 and FDR <0.05). (C) Functional categories of significant gene 743 hits determining fitness during challenge with 0.09-0.1 µg/ml ciprofloxacin. Information from 744 KEGG and UniProt functional annotations and from orthologs in well-studied reference species 745 were used to place genes into the listed broad categories.

746

747 Fig. 2. Magnitude of growth impairment is predicted by the severity of the Tn-seq fitness **defect.** (A) Tn-seq fitness profiles of transposon mutant pools constructed in a $gyrA^{WT}parC^{WT}$ 748 749 strain. Pools were grown without or with ciprofloxacin at 0.09-0.1 µg/ml. Bars show fitness 750 values of each transposon mutant at the indicated locus across all tested pools. (B) Growth of 751 pure cultures of WT or the indicated mutant in the absence or presence of ciprofloxacin (0.09 752 μ g/ml for Δ *ctpA* and *pbp1A*, 0.1 μ g/ml for Δ *adeIJK* and Δ *recN*, and 0.15 μ g/ml for Δ *gidA*). The 753 *pbp1a* mutant tested was *pbp1a*(N178TfsX27). Data points show geometric mean \pm SD (n = 3). 754 Cip, ciprofloxacin.

755

Fig. 3. Acquisition of *gyrA* resistance allele dramatically alters *A. baumannii* Tn-seq profile
 during ciprofloxacin challenge. (A) Transposon pools constructed in strains harboring

758	resistance alleles in gyrA or both gyrA and parC require increasing concentrations of					
759	ciprofloxacin to result in growth inhibition. Growth rate inhibition relative to untreated pools was					
760	plotted as in Fig. 1A. $gyrA^{WT}parC^{WT}$ growth data are from identical experiment shown in Fig.					
761	1A and are displayed to allow comparison to behavior of drug resistant mutants. Data points					
762	show average \pm SD (n \geq 2). Samples from cultures with 30-40% growth inhibition (dotted lines)					
763	were processed for Tn-seq. (B) Location of prophage regions (P1-P3) on A. baumannii 17978-					
764	mff chromosome map. Prophage positions were identified by using the PHASTER database (66).					
765	(C-F) gyrA resistance allele influences Tn-seq fitness profiles associated with ciprofloxacin					
766	stress. Mutant pools were challenged with drug concentrations that resulted in equivalent 30-					
767	40% growth inhibition [gyrA ^R , 1.1 µg/ml; gyrA ^R parC ^R , 13-14 µg/ml]. (C, E) Tn-seq fitness					
768	scores for each chromosomal gene with the indicated strain were calculated and visualized as in					
769	Fig. 1B (leftmost subpanel). Middle and rightmost subpanels show the identical dataset, with					
770	highlighting of loci for which knockout causes ciprofloxacin hypersensitization in the WT					
771	genetic background (green), or loci within prophages (color indicated in key). (D, F) Gene hits					
772	associated with significant changes in fitness during treatment were placed into functional					
773	categories as in Fig. 1C. Tn-seq hits resulting from $gyrA^R$ libraries treated with ciprofloxacin are					
774	enriched in prophage genes (F). (G) Tn-seq fitness scores resulting from ciprofloxacin challenge					
775	show genome positional bias that is greatly amplified in gyrA ^R mutant pools. Average per-gene					
776	Tn-seq fitness values are plotted in order of gene position on the chromosome or on plasmids					
777	pAB1-3. Boundaries of prophage regions (P1-P3) are indicated by vertical dotted lines. Top, no					
778	drug control. Bottom, ciprofloxacin was added at the concentrations indicated in panel A					
779	resulting in 30-40% inhibition (WT, 0.09-0.1 µg/ml; gyrA ^R , 1.1 µg/ml; gyrA ^R parC ^R , 13-14					

780 μ g/ml). (H) Expanded view of per-gene Tn-seq fitness scores in regions surrounding prophages 781 P1 and P3 for *gyrA*^R mutant treated with 1.1 μ g/ml ciprofloxacin.

782

783 Fig. 4. Ciprofloxacin-induced amplification of prophage DNA in strains harboring the

784 *gyrA*^R single-step resistance genotype. (A) Pure cultures of strains of the indicated genotype

785 were challenged with graded ciprofloxacin doses resulting in four levels of growth inhibition

786 (Roman numerals). (B) DNA content from each culture was analyzed by deep sequencing. x-axis

787 indicates nucleotide position along the *A. baumannii* ATCC17978-mff chromosome. y-axis

indicates normalized read depth (0-140 counts per million). Boundaries of prophage regions P1-3

are indicated in red. Roman numerals indicate the level of growth inhibition caused by

representative of two independent experiments. (C) Expanded view of

300kb window showing amplification of genomic regions surrounding prophages P1 and P3. Y-

axis indicates normalized sequencing read depth (0-160 counts per million).

793

794 Fig. 5. Ciprofloxacin challenge results in activation of prophage gene expression that is heightened in $gyrA^{R}$ -single mutants. (A) Strains of the indicated genotype were challenged 795 796 with ciprofloxacin concentrations that resulted in two levels of growth inhibition relative to no 797 treatment (i, ~45% growth inhibition; ii, ~70% growth inhibition). Data points show average \pm 798 SD (n = 3). (B). RNA-seq transcriptional profiles of panel A cultures. Fold change (log2) of each 799 gene (treated vs untreated) was plotted in order of position on the chromosome or plasmids 800 (pAB1-3). rRNA and tRNA genes were excluded from RNA-seq analysis, resulting in different 801 gene number assignments as compared to those in Fig. 3D. Boundaries of prophage regions P1-3 802 are denoted by vertical dotted lines. Roman numerals indicate growth inhibition level. (C)

803 Expanded views of RNA-seq log2-fold change ratios for genes surrounding P1-3 in $gyrA^{R}$ -single 804 mutant (condition *ii*, ciprofloxacin 1.1µg/ml).

805

Fig. 6. Enhanced SOS response induction in $gyrA^{R}$ -single mutants exposed to ciprofloxacin. 806 807 (A-B) SOS response genes are induced during growth with ciprofloxacin. (A) RNA-seq data 808 reveal DNA damage/SOS response induction during growth with ciprofloxacin. Bars show log2 809 fold change \pm SEM (n = 3) for WT or gyrA^R-single mutant treated with ciprofloxacin 810 concentrations resulting in ~70% growth inhibition (condition *ii* from Fig. 5). *, p<0.05, 811 unpaired t test. (B) Location of DNA damage/SOS response genes induced in $gyrA^{R}$ -single 812 mutant strain. x-axis indicates gene position along the A. baumannii chromosome, y-axis indicates the log2 fold change (Cip 1.1 μ g/ml vs untreated, gyrA^R-single mutant) from previously 813 814 presented RNA-seq data. (C-D) Fluorescence reporter assays demonstrate enhanced recA gene expression in $gyrA^{R}$ -single mutant. Strains of the indicated genotype harboring (C) pCC1 815 816 (mKate2 fusion to recA promoter plus 5' untranslated region (UTR)) or (D) pCC7 (trpB 817 promoter replacing recA promoter in pCC1) were cultured as in RNA-seq experiments. Growth 818 inhibition relative to untreated control was calculated (top). Average mKate2 intensity per cell 819 within each sample was measured by fluorescence microscopy, and median fluorescence values 820 of the population were determined (bottom). Data points represent the average inhibition values 821 (top) or average of median fluorescence values (bottom) \pm SD from $n \ge 2$ biological replicates 822 pooled from multiple independent experiments. Dotted lines denote fluorescence intensity of 823 untreated samples.

824

Fig. 7. Model for resistance allele-dependent prophage amplification in *A. baumannii*

826 exposed to sub-MIC fluoroquinolone stress. The model posits that prophage DNA replication 827 depends on host DNA gyrase activity. (A) In WT cells, both gyrase (GyrA) and topo IV (ParC) 828 are drug sensitive. Gyrase, which has higher affinity for CIP (blue triangles), is effectively 829 targeted by the drug. Ciprofloxacin-corrupted gyrase results in double-strand DNA breaks that 830 signal derepression of prophage gene expression. Prophage DNA replication cannot proceed, however, because gyrase function is blocked. (B) In single $gyrA^R$ mutant cells, topo IV/ParC has 831 higher affinity for ciprofloxacin than the resistant gyrase and is the effective drug target. Topo IV 832 833 corruption results in a robust DNA damage response and activation of prophage gene expression, 834 and gyrase-dependent prophage replication (prophages 1 and 3) proceeds because GyrA is not

835 drug-inhibited. (C) In double $gyrA^{R}parC^{R}$ mutant cells growing at high drug concentrations,

836 GyrA again has relatively higher affinity for ciprofloxacin than ParC and becomes the effective

target despite the S81L drug binding site alteration. The resulting DNA lesions induce the SOS

response and prophage gene expression, but prophage replication does not proceed efficiently

839 because gyrase function is again blocked.

840

- 841 Supplemental Figure Legends
- 842
- 843 Fig. S1. pDL1073 feature map.

844

Fig. S2. Sub-MIC ciprofloxacin treatment of *A. baumannii* with gyrA^{WT} and parC^{WT} alleles
does not significantly alter Tn-seq fitness values assigned to prophage region genes. (A) The
Tn-seq dataset shown in Fig. 1B (WT background +/- treatment with ciprofloxacin 0.09-0.1

µg/ml) was reanalyzed to highlight fitness values associated with genes within prophage regions
P1-P3. Prophages regions are highlighted with color indicated in the key.

850

Fig. S3. Comparison of transcription levels between ciprofloxacin-treated cultures of WT and $gyrA^{R}$ reveals enhanced prophage gene expression in the $gyrA^{R}$ single mutant. Strains were grown in the absence or presence of ciprofloxacin at concentrations shown in Fig. 5A, and RNA-seq data were analyzed such that WT and $gyrA^{R}$ strains were directly compared at each condition. Plots show log2 fold change (WT vs $gyrA^{R}$) of each gene in order of position on the chromosome or plasmids (pAB1-3).

857

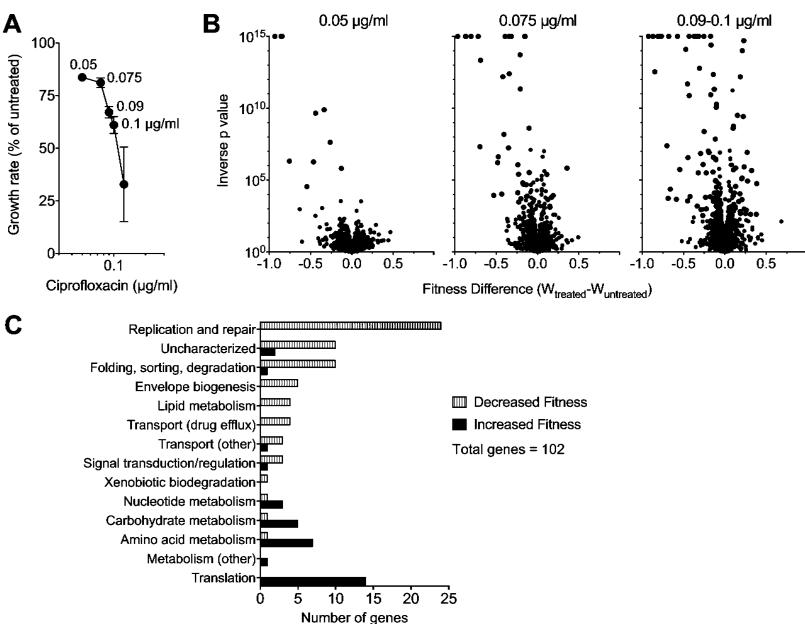
858 Fig. S4. Fluorescence microscopy analysis of SOS response in individual cells subjected to 859 **ciprofloxacin**. Strains harboring *recA-mKate2* were cultured and analyzed by fluorescence 860 microscopy as described in legend to Fig. 6C. (A) Phase contrast (rows 1 and 3) and fluorescence 861 (rows 2 and 4) microscopy images from one representative experiment used to quantify recA-862 *mKate2* signal in Fig. 6C. Cells of the indicated genotype were treated with the noted 863 concentration of ciprofloxacin resulting in similar degrees of growth inhibition (see panel C, 864 bottom three growth inhibition data points). (B) Population fluorescence analysis from one 865 representative experiment contributing to Fig. 6C quantifying SOS response to increasing 866 ciprofloxacin dose in different strain backgrounds harboring *recA-mKate2*. In the same 867 experiment shown in panel A, 4 different ciprofloxacin concentrations were tested per strain. 868 Average mKate2 intensity per cell was measured by fluorescence microscopy. Each data point 869 represents average fluorescence intensity of a single cell (at least 100 cells per condition were

- 870 analyzed). Bars indicate median values. (C) Growth inhibition relative to untreated control
- 871 resulting from the ciprofloxacin exposures in the representative experiment shown in panel B.

- **Table S1.** Bacterial strains and plasmids used in this study.
- **Table S2.** Oligonucleotide primers used in this study.
- **Data Set S1.** Tn-seq fitness data WT.
- **Data Set S2.** Tn-seq fitness data $gyrA^{R}$.
- **Data Set S3.** Tn-seq fitness data $gyrA^{R} parC^{R}$.
- 878 Data Set S4. RNA-seq data.

Table 1. Minimal Inhibitory Concentration (μ g/ml) of Ciprofloxacin with WT and mutant *A. baumannii*.

	amino ac	id change:	ciprofloxacin MIC (µg/ml)
strain	GyrA	ParC	
WT	-	-	0.25
gyrA ^R	S81L	-	2
gyrA ^R parC ^R	-	S84L	0.25
gyrA ^R parC ^R	S81L	S84L	32



bioRxiv preprint doi: https://doi.org/10.1101/442681; this version posted October 14, 2018. The copyright holder for this preprint (which was not certified by peer review) is the author/funder. All rights reserved. No reuse allowed without permission.

